VNU Journal of Science: Natural Sciences and Technology, Vol. 39, No. 4 (2023) 46-56

VNU Journal of Science: Natural Sciences and Technology

Journal homepage: https://js.vnu.edu.vn/NST

Original Article

N-TiO_2/FeMIL-88B- A Promising Photocatalyst for Photoconversion of CO_2 into Methanol

Phung Thi Lan[1], Nguyen Hoang Hao[2], Nguyen Van Thuc[3], Nguyen Ngoc Ha[4], Le Minh Cam[1], Nguyen Thi Thu Ha[1,*]

[1]*Hanoi National University of Education, 136 Xuan Thuy, Cau Giay, Hanoi, Vietnam*
[2]*College of Education, Vinh University, 182 Le Duan, Vinh, Vietnam*
[3]*VNU University of Science, 19 Le Thanh Tong, Hoan Kiem, Hanoi, Vietnam*
[4]*Vietnam Education Quality Management Agency, Ministry of Education and Training, 35 Dai Co Viet, Hanoi, Vietnam*

Received 21 August 2023
Revised 09 October 2023; Accepted 02 November 2023

Abstract: The present objective of this work is to find photoactive materials capable of facilitating visible light-driven redox reactions between CO_2 and H_2O. Our research is primarily focused on the incorporation of nitrogen (N) into the crystal lattice of titanium dioxide (TiO_2) and its deposition onto Fe-MIL-88B to improve light absorption properties, minimize recombination of photo-generated electron-hole pairs, and increase CO_2 adsorption capacity. The N-TiO_2/Fe-MIL-88B composite was successfully prepared and characterized using SEM, XRD, and EDX techniques. The introduction of N-TiO_2 into Fe-MIL-88B does not damage the crystal structure of Fe-MIL-88B. Anatase is the only crystalline phase observed from the XRD diffraction pattern. SEM images show that N-TiO_2 is well dispersed on the Fe-MIL-88B surface. The results of quantum simulations indicate that TiO_2 strongly interacts with Fe-MIL-88B. The binding energy is determined to be -78.2 kcal/mol. The calculated UV-Vis results revealed that the light absorption edge of the TiO_2/Fe-MIL-88B was redshifted compared to that of the pure TiO_2 (from ca. 500 nm to 550 nm). The redshifted light absorption of TiO_2/FeMIL-88B suggests that the band gap of TiO_2/Fe-MIL-88B is narrower compared to that of the pristine TiO_2, indicating the better light utilization ability of the TiO_2/Fe-MIL-88B. Results from high-performance liquid chromatography show that N-TiO_2 can convert CO_2, but at a significantly low rate. The methanol formation is distinctly observed only over the N-TiO_2/Fe-MIL-88B catalyst. The CO_2 conversion efficiency, estimated using gas chromatography, is calculated to be 11.94%.

Keywords: TiO_2, Fe-MIL-88B, photosynthesis, CO_2 conversion, methanol, MOFs.

* Corresponding author.
E-mail address: ntt.ha@hnue.edu.vn

https://doi.org/10.25073/2588-1140/vnunst.5597

1. Introduction

The increased use of fossil fuels results in an explosive increase in CO_2 emissions into the atmosphere, causing environmental problems such as global warming and detrimental environmental pollution. Therefore, searching for renewable and environmentally friendly energy resources has turned out to be an urgent task for the long-term development of human society. Because solar energy is considered one of the most inexhaustible and green energy sources, much attention has been paid to the conversion of incoming solar energy into valuable solar fuels [1]. Among various possibilities, artificial photosynthesis, or photocatalytic CO_2 reduction into green solar fuels such as CH_4, HCO_2H, CH_2O, and CH_3OH, has been known as one of the most promising technologies because it can simultaneously produce valuable solar fuels and imitate the CO_2 concentration in the atmosphere. To achieve this objective reaction, many efforts have been devoted to developing efficient photocatalysts ranging from semiconducting materials, such as TiO_2, Zn_2GaO_4, CdS, and C_3N_4 [2], to metal–organic frameworks (MOFs), including NH_2-MIL-125(Ti) [3], Fe-MOF-525 [4], or Mn(bpydc)-$(CO)_3Br$ [5]. Due to its sufficiently high reduction potential, low cost, and high stability, TiO2 has attracted wide attention as one of the most potential photocatalysts for CO_2 reduction [6]. However, due to its rapid electron-hole recombination, TiO2 suffers from low photoconversion efficiency for practical applications [7]. Moreover, attributing to its relatively large band gap energy, merely 5% of incoming solar light can be utilized by the bare TiO_2 for photocatalytic reactions [8]. Therefore, from a practical point of view, it is of great significance to improve the electron-hole separation efficiency and light utilization ability of TiO_2 [9]. One of the most widely applied approaches to preparing highly efficient TiO_2 for photocatalytic CO_2 reduction is the surface modification of TiO_2, such as impurity doping, metal deposition, alkali modification, heterojunction construction, and carbon-based material loading [10]. The dispersion of photocatalysts is noted to be another critical factor for efficient photoreduction of CO_2. Photocatalysts immobilized in the zeolite or MOF supports are usually highly dispersed. As a new family of inorganic-organic hybrid supramolecular materials, MOFs emerge as promising catalysts for CO_2 photoconversion due to their super-high surface area and excellent adsorption capacity for CO_2 molecules [11]. Our previous works [12] have shown the superb CO_2 adsorption capacity of MIL 88-B.

The present work focuses on doping nitrogen on the crystal lattice of TiO_2 and then depositing it onto Fe-MIL-88B for enhancement of light absorption properties, reduction of recombination of photo-generated electron-hole pairs, and also for the high adsorption CO_2 capacity of the material as well.

2. Experiments

2.1. Preparation of N-TiO_2/Fe-MIL-88B

2.1.1. The Fe-MIL-88B Synthesis

Fe-MIL-88B powder is first synthesized using the method described in [11, 12]: 1 mmol of $FeCl_3$ anhydrous is dissolved in 2 ml of DMF. 1 mmol of H_2BDC is dissolved in 8 ml of DMF (with the ratio of $FeCl_3$:H_2BDC: DMF = 1:1:10). Then two solutions are mixed and stirred for 4 hours. The mixture is crystalline in an autoclave at 100 °C for 24 hours. Finally, the obtained solid is filtered, washed with DMF, and dried in the air.

2.1.2. The N-TiO_2 Synthesis

N-TiO_2 is prepared through the hydrolysis of titanium tetrachloride and ammonium hydroxide. A typical reaction adds 5 mL of TiCl4 to 20 mL of absolute ethanol. Then, the solution is slowly dropped into 30 mL of deionized water under magnetic stirring (solution A). After cooling to room temperature, ammonia solution is added dropwise into solution A until pH = 7. Subsequently, 0.5497 g of urea (equivalent to

5% N/TiO_2 calculated from the reaction equation) is dissolved in 15 mL of ethanol and introduced into the above solution. The white viscous colloid is allowed to continue stirring for 1 hour at room temperature, then dried at 80 °C for 10 hours. Finally, the samples are calcined in the oven following the procedure: at 300 °C for 1 hour, at 400 °C for 1 hour, and at 500 °C for 3 hours.

2.1.3. The Synthesis of 5% (N-TiO_2)/Fe-MIL-88B

4.4 g of Fe-MIL-88B is ultrasonicated in 30 mL of DMF for 1.5 hours, then 0.22 g of N-TiO_2 is added to the suspension and continuously ultrasonicated for 1 hour. The mixture is finally heated to 80 °C for 2 hours, then dried in an oven overnight before being used. Following this procedure, approximately 5% by weight of N- TiO_2 is dispersed on Fe-MIL-88B.

2.2. Characterization

Powder X-ray diffraction (XRD) patterns are collected with Cu Kα radiation (λ = 1.5406 Å) in the range of $2\theta = 4^o \div 43^o$. The microstructures of the purified sample are characterized by scanning electron microscopy (SEM). Energy-dispersive X-ray (EDX) is employed for compositional analyses. The specific surface area and pore structures of the Fe-MIL-88B are determined from the physisorption of N_2 at 77K and a low relative pressure (P/P^0) of 0–0.3. The measurement is performed on a Tristar-3000 instrument. KBr solid-state FTIR is carried out to analyze the chemical function groups of the samples.

2.3. The Photocatalytic Activity Measurements

The photocatalytic activities are tested using a reactor system (Figure 1) built in the lab.

The CO_2 photoreduction process is conducted at ambient conditions (25 ± 5 ^{o}C, 1 bar) over the studied catalyst samples. The carbon dioxide gas employed in this study, originating from China, exhibits a high purity level of 99.9999%. Approximately 0.2 g of catalyst is evenly coated onto glass trees (glass rods) using double-sided tape with a dimension of 3.5 cm × 9.0 cm, which are then loaded into the quartz column. A xenon arc lamp (Model No. CHF XM500W) with a UV cut-off filter (λ > 400 nm) was employed throughout the study. The products are analyzed by HPLC (Shimadzu), a UV detector at 254 nm wavelength, using H_2O as a solvent at a flow rate of 0.75 mL/min and a sample volume of 10 μL.

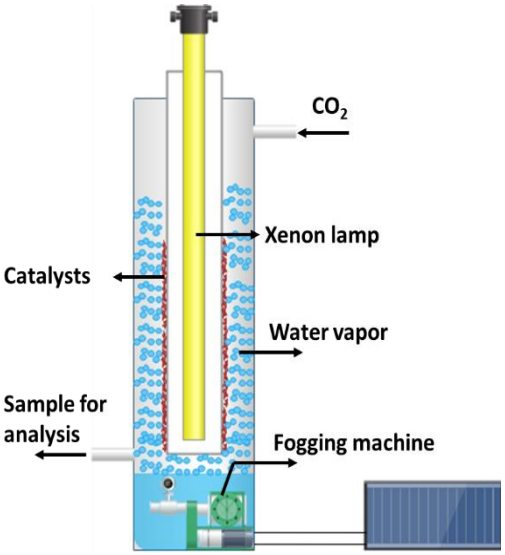

Figure 1. Schematic of the apparatus used for the photocatalytic reduction of CO_2 under visible light irradiation.

Leaks are tested by purging the photoreactor with helium. If leak-proof, the reactor is purged with this gas for one and a half hours, and the gas flow is changed to CO_2 gas. The CO_2 gas is saturated with water vapor for 30 minutes. After that, the light source is switched on. Following 4 hours of light irradiation, the production of fuels such as methanol, ethanol, or acetaldehyde will be observed from the photocatalytic reduction of vapor-phase CO_2 using water as a reductant under visible light.

2.4. Theoretical Calculations

A theoretical calculation is also performed to determine the interaction between TiO_2 and Fe-MIL-88B using the Density Functional Theory approach within the generalized

gradient approximation (GGA) implemented in the SIESTA code [13]. The Perdew, Burke, and Ernzerhof gradient-corrected function is used to calculate the exchange-correlation energy [14].

3. Results and Discussion

3.1. Characterization

Figure 2 introduces the SEM images of the synthesized MIL-Fe and N-TiO_2/Fe-MIL-88B samples. It is easy to see that Fe-MIL-88B has an octahedron crystal structure with uniform cubic symmetry.

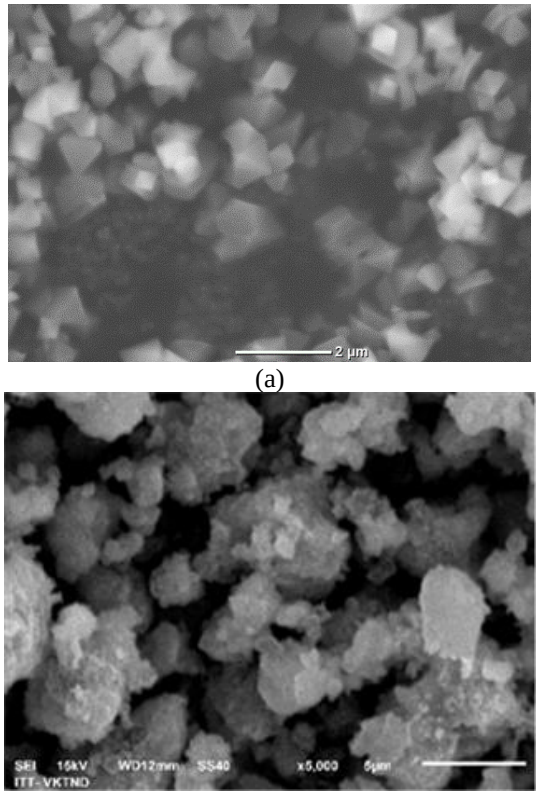

Figure 2. SEM of the synthesized Fe-Mil-88B (a) and N-TiO_2/Fe-MIL-88B.

The crystalline nanoparticles are about 500 nm in size and are discrete, non-clustered. This result is consistent with the published results on MIL-88B [11] and indicates that Fe-MIL-88B has been successfully synthesized. The introduction of N-TiO_2 does not damage the crystal structure of Fe-MIL-88B. The N-TiO_2 clusters of 30 ÷ 50 nm in size are evenly dispersed on the surface of Fe-MIL-88B.

In Figure 3, the FT-IR spectrum of the synthesized material with the main spectral fringes agrees with the published IR spectrum for this material. There is no spectral pattern on the spectrum corresponding to the wave number of 1700 cm^{-1}, which is typical for the free BDC ligand. The strong oscillation at wave number 1392.61 cm^{-1} is attributed to the vibration of the C-C bond in the benzene ring. A strong and obtuse fringe at 3425.58 cm^{-1} characterizes the oscillation of the O-H bond. The peak corresponding to wave number 1658.78 cm^{-1} characterizes DMF, and Fe3(µ3-O) oscillation corresponds to the spectral fringe at 624.9 cm^{-1}.

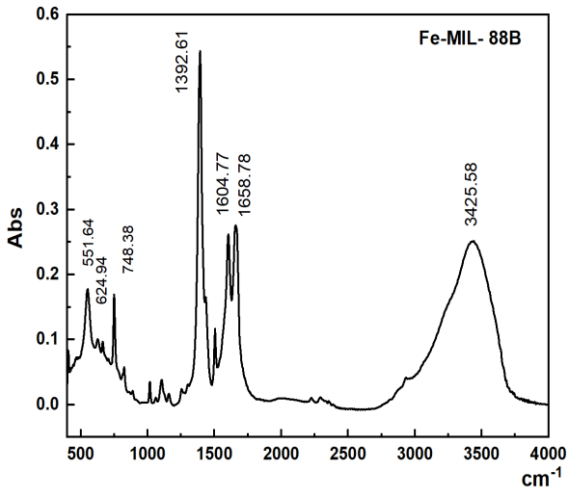

Figure 3. FTIR spectrum of Fe-MIL-88B.

Figure 4 is the X-ray diffraction of the Fe-MIL-88B sample. The XRD patterns confirm the MIL-88B structure. The characteristic peaks for MIL-88B, which appear at angles of 2θ = 9.34°, 10.50°, 18.86°, and 22.05° are consistent with the previous studies [11]. The XRD pattern also shows that the synthesized MIL-88B material has high crystallinity, and no characteristic peak for Fe_2O_3 is detected.

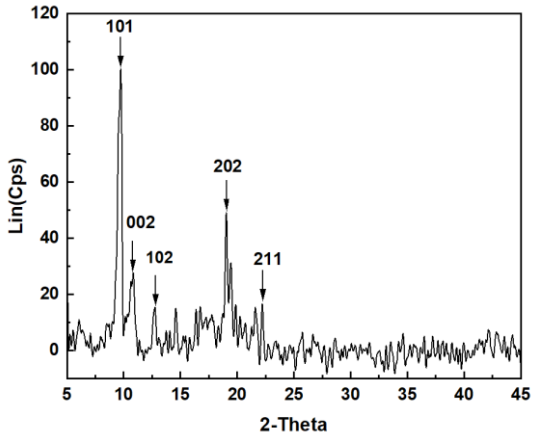

Figure 4. XRD pattern of Fe-MIL-88B.

N-TiO_2/Fe-MIL-88B was prepared and characterized using SEM, XRD, and EDX. Figure 5 presents the XRD patterns of TiO_2 and N-TiO_2/Fe-MIL-88B.

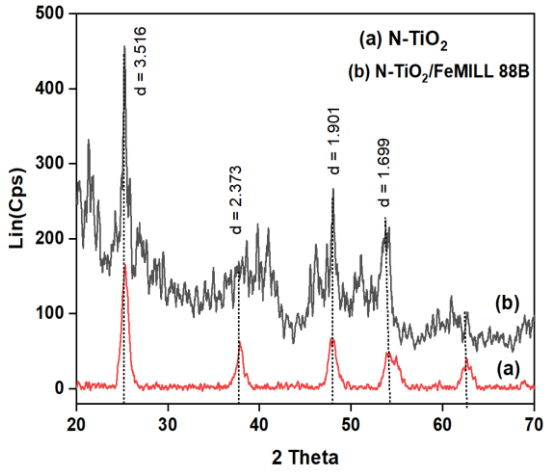

Figure 5. XRD pattern of N-TiO_2 (a); and N-TiO_2/Fe-MIL-88B (b).

In the XRD pattern (a), peaks corresponding to TiO_2 appear at 2 theta (2θ) = 25°, 37°, 38°, and 48°. The anatase is the only crystalline phase observed after calcination at 400 °C. No diffraction peak for the nitrogen is observed. The XRD pattern of N-TiO_2/Fe-MIL-88B (b) looks similar to that of TiO_2, except that the peaks are not sharp, and one peak appears at the position of 2 theta = 22.05^0, which is assigned to Fe-MIL-88B.

The N_2 adsorption-desorption isotherms at 77K of the synthesized material samples are presented in Figure 6, and the textile properties of the surfaces are shown in Table 1. From Figure 6, it can be seen that on the linear scale of relative pressure (p/p°), the curve has an I–form according to the IUPAC classification [15], proving that the synthesized Fe-MIL-88B belongs to the category of nanoporous materials. The nanopore volume is 0.1106 cm^3/g, containing very few mesopores. The specific surface area, according to BET is 150 m^2/g but is predominantly internal surface area (accounting for 87% of the total surface area of the sample).

The studied sample is shown to belong to a mesoporous material with a concentrated pore width of 13 nm and does not contain large pores. The dispersion of N-TiO_2 on the surface of Fe-MIL, forming small clusters (from the SEM image), significantly reduces the specific surface area and total volume of Fe-MIL-88B.

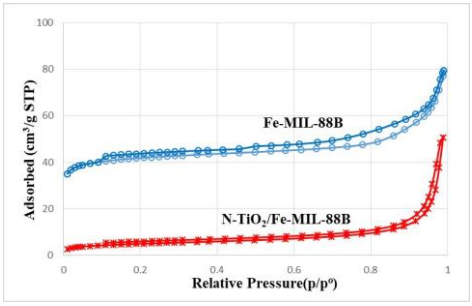

Figure 6. The N_2 adsorption isotherm at 77K for the synthesized material samples.

Table 1. The surface areas and the porous characterization of Fe-MIL-88B and N-TiO_2/Fe-MIL-88B

Sample	Fe-MIL-88B	N-TiO_2/Fe-MIL-88B
S_{BET} (m^2/g)	150 ± 2	18 ± 1.5
S_{ex} (m^2/g)	18 ± 1.5	12 ± 1.5
S_{mic} (m^2/g)	131 ± 2	6 ± 1.0
V_{BJH} (cm^3/g)	0.0607	0.0701
V_{mic} (cm^3/g)	0.0569	0.0027
D (nm)	13,2837	24.2590

The chemical composition of the synthesized samples is analyzed by the EDX technique. Figure 7 and Table 2 show the EDX spectra of TiO_2 (a) and N-TiO_2/Fe-MIL-88B (b). The results indicate the right composition of the synthesized samples. In the EDX spectrum of N-TiO_2/Fe-MIL-88B, the nitrogen component is not detected. This can be explained by the fact that nitrogen produces a feeble response and is also limited by the detector design. Scanning electron microscopy with energy dispersive X-ray spectrometry (SEM-EDS) is an elemental microanalysis method widely applied. However, one of the limitations of this technique is in the field of low Z element detection due to the X-ray absorption phenomenon, which occurs due to the Be window of the detector. X-ray absorption is a function of the energy of X-rays. Low-energy peaks will be more strongly absorbed than high-energy ones. Therefore, an unreliable detection is observed for N_2 for most materials.

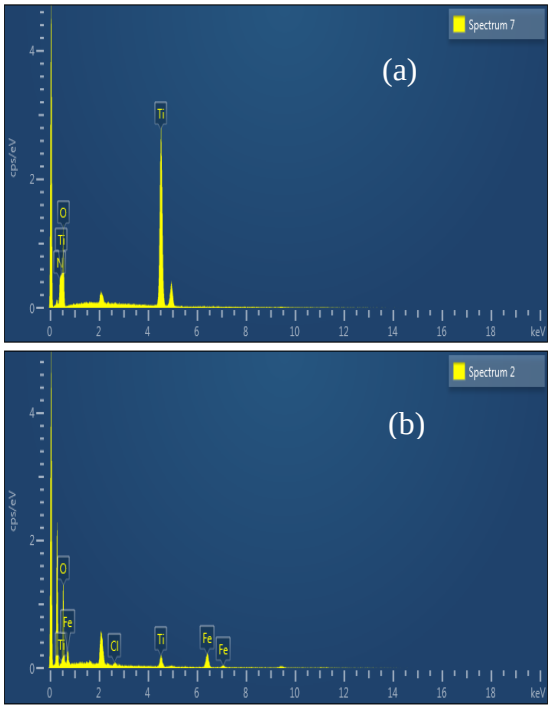

Figure 7. The EDX spectra of the TiO_2 (a) and N-TiO_2/Fe-MIL-88B (b).

Table 2. The main elements' composition of TiO_2 and N-TiO_2/Fe-MIL-88B analyzed by the EDX technique

Elements (%wt)	TiO_2	N-TiO_2/Fe-MIL-88B
C	2.54	50.87
O	49.98	35.64
Fe	-	10.04
Ti	47.48	3.15

3.2. The Evidences for the Present of Nitrogen in N-TiO_2

The role of nitrogen is known to reduce the band gap energy of TiO_2, enabling TiO_2 to perform effectively in the visible light range [16]. Therefore, in this study, the presence of nitrogen in the N-TiO_2 sample is evidenced through UV-vis DRS spectra (Figure 8) and XRD patterns (Figure 9). It has been demonstrated that doping TiO_2 with nitrogen narrows the band gap compared with pristine TiO_2. The nitrogen atoms doping into the crystal structure of TiO_2 modify the electronic band structure of TiO_2, leading to the formation of new mid-gap N 2p energy band levels above the O 2p valance band, suppressing the recombination of photo-generated charge carriers [17]. The absorption spectrum of N-TiO_2 (Figure 8) shows a significant shift towards longer wavelengths compared to that of TiO_2. Using the Kubelka-Munk equation:

$$(A.h\vartheta)^{1/2} = A(h\vartheta - E_g)$$

The band gap energies are calculated for TiO_2 and N-TiO_2, resulting in values of 2.9 eV and 2.2 eV for TiO_2 and N-TiO_2, respectively. These results suggest that TiO_2 doped with a small amount of nitrogen has the ability to operate in the visible light range. Another characteristic indicating the presence of nitrogen in N-TiO_2 is the XRD pattern (Figure 9). The synthesis procedure used in the study results in the domination of the rutile crystal structure of TiO_2 (>90%); however, the presence of nitrogen in the TiO_2 sample prevents the phase

transition from anatase to rutile. The XRD pattern of N-TiO_2 shows that the anatase crystalline phase constitutes 75%. Anatase is known to be the most catalytically active form among the three polymorphs of TiO_2.

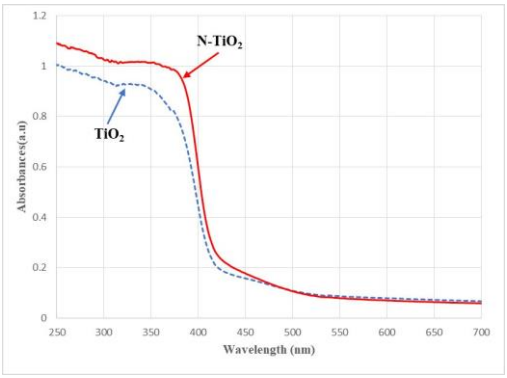

Figure 8. UV-visible Diffuse Reflectance spectra of synthesized samples: TiO_2 and N-TiO_2.

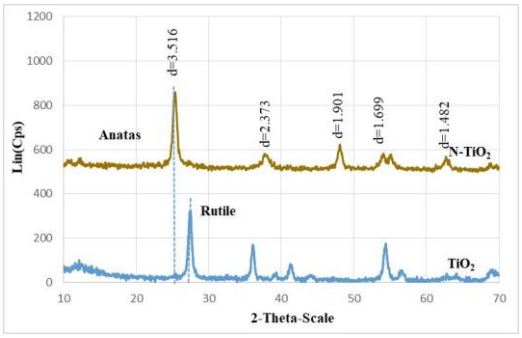

Figure 9. XRD patterns of synthesized samples: TiO_2 and N-TiO_2.

3.3. Theoretical Study on the Interaction between Nano TiO_2 and Fe-MIL-88B

The obtained characteristic results show that N-TiO_2 is successfully dispersed on the surface of the Fe-MIL-88B material. However, the nature of the interaction between TiO_2 and Fe-MIL-88B needs to be clarified: is the process of bringing TiO_2 to MIL-88B a physical mixing process? Or is TiO_2 bound and "adsorbed" on the MIL-88B? If yes, then what is the type of interaction? This can be explained by calculating the interaction energy between TiO_2 nanoparticles and the Fe-MIL-88B material. Figure 10 illustrates the optimized TiO2/Fe-MIL-88B structure at the GGA/PBE level of theory. The cluster $(TiO_2)_7$ is chosen to represent the TiO_2 nanoparticles.

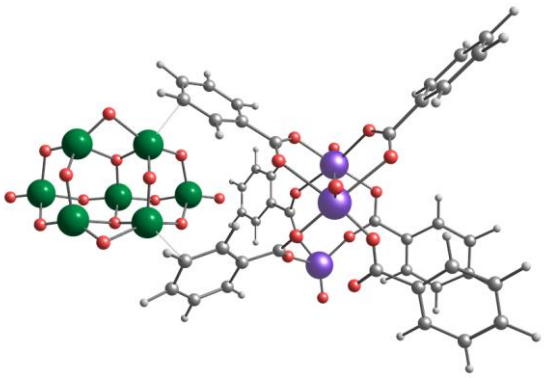

Figure 10. Optimized structure of TiO_2/Fe-MIL-88B.

The interaction energy between TiO_2 and Fe-MIL-88B is calculated by the equation:

$E_{bind} = E(TiO_2/Fe\text{-}MIL) - E(TiO_2) - E(Fe\text{-}MIL)$

Where $E(TiO_2/Fe\text{-}MIL)$, $E(TiO_2)$, $E(Fe\text{-}MIL)$ are energies of TiO_2/Fe-MIL-88B, TiO_2, and Fe-MIL-88B, respectively.

The E_{bind} is obtained to be –78.2 kcal/mol. This relatively negative value indicates that TiO_2 is strongly adsorbed on MIL-88B. The adsorption force is chemical due to the formation of weak TiO_2 bonds with the C atoms of the benzene ring. This is completely beneficial for the subsequent CO_2 photocatalytic conversion because: i) nano TiO_2 is stabilized and stable, and is well dispersed on Fe-MIL-88B; ii) the interaction between TiO_2 - C atoms (of the benzene ring) can lead to a decrease in the band gap of TiO_2, which means that the absorbed light wavelength suitable for photocatalytic conversion will shift to the visible region (the redshift). At the same time, it reduces the recombination of photo-generated electrons and holes, which are the active centers in the photocatalytic reaction.

Indeed, the calculated UV-Vis results reveal that the light absorption edge of the TiO_2/FeMIL-88B is redshifted compared to that of the pure TiO_2 (from *ca.* 500 nm to 550 nm, Figure 11). The redshifted light absorption of TiO_2/Fe-MIL-88B suggests that the bandgap of

TiO_2/Fe-MIL-88B is smaller than that of pristine TiO_2, indicating the better light utilization ability of TiO_2/Fe-MIL-88B. Besides, the light absorption intensity of TiO_2/Fe-MIL-88B at 550 nm is three times higher than that of nano TiO_2 at 500 nm. Thus, putting TiO_2 on Fe-MIL-88B will be more favorable for the photocatalytic CO_2 conversion.

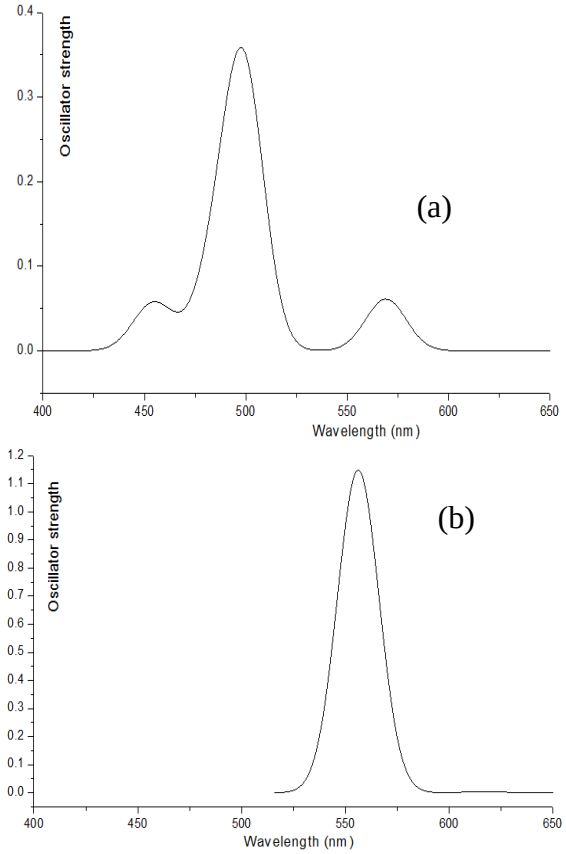

Figure 11. Calculated UV-Vis for pristine TiO_2 (a) and TiO_2/Fe-MIL-88B (b).

3.4. Photocatalytic Reduction of CO_2 to Methanol using H_2O as Reductant

Before photocatalytic experiments, the blank test is conducted to confirm that the reaction between CO2 and water vapor cannot occur without a catalyst. Three samples were tested for their catalytic activity in the photoreaction of CO_2 and H_2O: pure TiO_2, N-TiO_2, and N-TiO_2/Fe-MIL-88B. Following 4 hours of light irradiation, methanol is observed from the photocatalytic reduction of vapor-phase CO_2 using water as a reductant under visible light. The observed HPLC data is presented in Figure 12. The plot (a) is the HPLC of deionized water. No peak for methanol formation is observed if the reaction mixture is exposed to Fe-MIL-88B alone (plot b). TiO_2 can convert CO_2, but with a very low rate and low efficiency (plot c). Results from HPLC show that N-TiO_2 can convert CO_2, but at a very low rate (plot d). Only over N-TiO_2/Fe-MIL-88B (plot e) can the methanol formation be observed with the CO2 conversion efficiency of 11.94%, estimated using gas chromatography (GC). This high photocatalytic CO_2 reduction activity of the N-TiO_2/Fe-MIL-88B sample compared to that of the pristine TiO_2 and N-TiO_2 under visible light irradiation is attributed to the better light absorption ability of N-TiO_2/Fe-MIL-88B and also the high CO_2 adsorption capacity of Fe-MIL-88B.

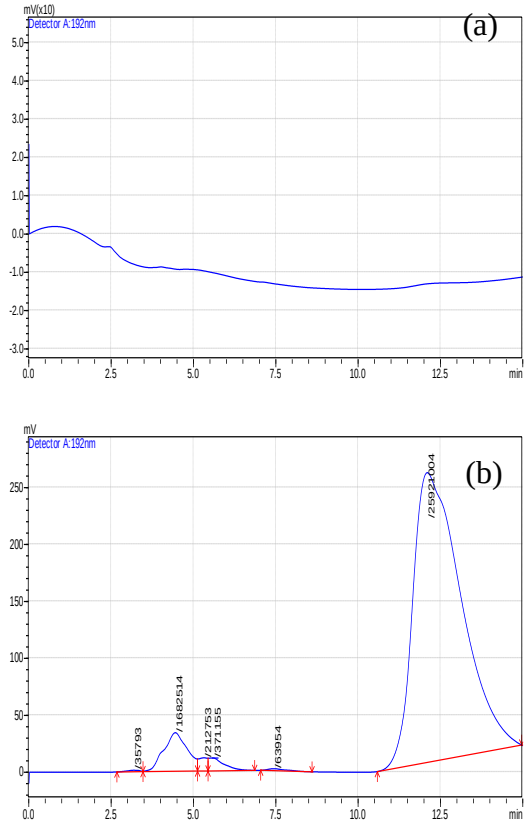

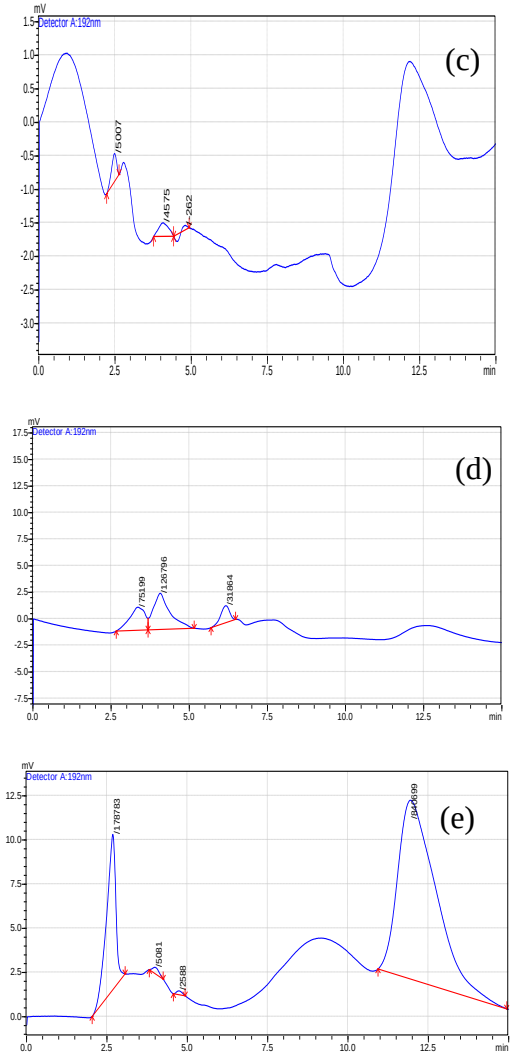

Figure 12. HPLC spectra of reactions mixture in liquid phase after 4 hours exposed under visible light (a) deionized water, (b) Fe-MIL-88B, (c)TiO_2, (d) N-TiO_2, (e)N-TiO_2/Fe-MIL-88B.

Table 3. The analyzed HPLC results of H_2O, MIL88B, TiO_2, N-TiO_2 and 5% N-TiO_2/ MIL88B

Samples	Ret. Time (min)	Peak area
H_2O		0
Fe-MIL-88B	2.75	0.0
TiO_2	2.50	5007
N-TiO_2	2.50	75199
N-TiO_2/Fe-MIL-88B	2.75	178783

The CO_2 conversion efficiency of the N-TiO_2/Fe-MIL-88B composite is determined by gas chromatography. By comparing the peak area of the starting material sample containing the gases (CO_2, O_2, and N_2) with that of the post-reaction sample, the conversion efficiency is calculated according to the equation:

$$\%CO_2 = \frac{S(before) - S(after)}{S(before)}$$

Where S(before) is the peak area of the feed before going through the catalyst, and S(after) is the peak area of the gas stream after leaving the catalyst. The spectra (Figure 13) showed no peaks other than three O_2, N_2, and CO_2 peaks, showing that the reaction did not produce gas products. The calculated results are presented in Table 4.

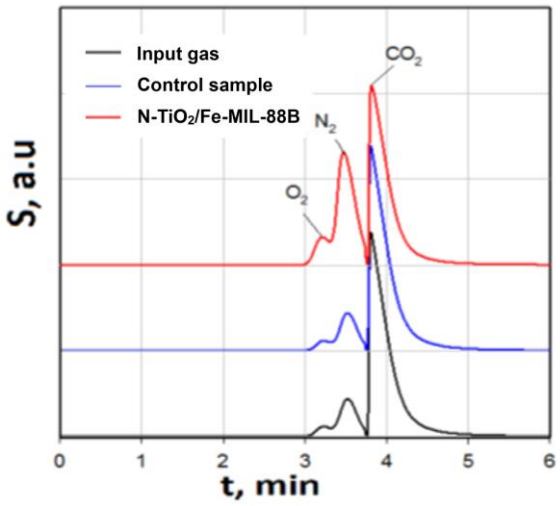

Figure 13. Change in the gas mixture composition before and after exposing 4 hours under visible light (results from analyzing GC spectra).

Table 4. The peak's areas (S) result from the GC spectra

Samples	S (a.u)	%CO_2 conversion
Feed (before)	1.97×10^8	0.00
Reference	1.97×10^8	0.00
After exposing over N-TiO_2/Fe-MIL-88B	1.73×10^8	11.94

The CO_2 conversion efficiency is relatively high (11.94%) compared to previous studies. Thus, it can be concluded that modifying TiO_2 and combining it with Fe-MIL-88B will create an effective material for CO_2 photocatalytic conversion.

4. Conclusion

Fe-MIL-88B has been successfully synthesized. The FTIR analysis of the sample agrees with the suggested Fe-MIL-88B formula. The XRD patterns of the sample confirm the MIL-88B structure. N-TiO_2/Fe-MIL-88B was prepared and characterized using SEM, XRD, BET, and EDX. The introduction of N-TiO_2 cannot damage the crystal structure of Fe-MIL-88B. In the XRD pattern, peaks corresponding to TiO_2 appear at $2\theta = 25^o$, 37^o, 38^o, and 48^o. Anatase was the only crystalline phase observed from the XRD diffraction pattern. Quantum simulation has been used to study the interaction between TiO_2 and the support Fe-MIL-88B. The calculated UV-Vis results revealed that the light absorption edge of the TiO_2/Fe-MIL-88B was redshifted compared to that of the pure TiO_2. The redshifted light absorption of TiO_2/Fe-MIL-88B suggests that the band gap of TiO_2/Fe-MIL-88B is smaller than that of the pristine TiO_2, indicating the better light utilization ability of the TiO_2/Fe-MIL-88B. Three samples were tested for their catalytic activity in the photoreaction of CO_2 and H_2O: pure TiO_2, N-TiO_2 and N-TiO_2/Fe-MIL-88B. The results from HPLC spectra reveal that TiO_2 and N-TiO_2 can convert CO_2 but at a very low rate. Only over N-TiO_2/Fe-MIL-88B, the methanol formation can be observed with the CO_2 conversion efficiency of 11.94%, which was estimated using gas chromatography. This high photocatalytic CO_2 reduction activity of the N-TiO_2/Fe-MIL-88B sample compared to that of the pristine TiO_2 and N-TiO_2 under visible light irradiation is attributed to the better light absorption ability of N-TiO_2/Fe-MIL-88B and also the high CO_2 adsorption capacity of Fe-MIL-88B.

Acknowledgements

This research is funded by Vietnam National Foundation for Science and Technology Development (NAFOSTED) under grant number 104.06-2020.48.

References

[1] J. Jiao, Y. Wei, K. Chi, Z. Zhao, A. Duan, J. Liu, G. Jiang, Y. Wang, X. Wang, C. Han, P. Zheng, Platinum Nanoparticles Supported on TiO_2 Photonic Crystals as Highly Active Photocatalyst for the Reduction of CO_2 in the Presence of Water, Energy Technology, Vol. 5, 2017, pp. 877 - 883

[2] A. J. Bard, M. A. Fox, Artificial Photosynthesis: Solar Splitting of Water to Hydrogen and Oxygen, Acc. Chem. Res, Vol. 28, 1995, pp. 141-145.

[3] M. Aresta, A. Dibenedetto, Tilisation of CO_2 as a Chemical Feedstock: Opportunities and Challenges, Dalton. Trans, Vol. 28, 2007, pp. 2975-2992.

[4] M. Halmann, Photoelectrochemical Reduction of Aqueous Carbon Dioxide on P-type Gallium Phosphide in Liquid Junction Solar Cells, Nature, Vol. 275, 1978, pp. 115-116.

[5] T. Inoue, A. Fujishima, S. Konishi, K. Honda, Photoelectrocatalytic Reduction of Carbon Dioxide in Aqueous Suspensions of Semiconductor Powders, Nature, Vol. 277, 1979, pp. 637-638.

[6] M. Tahir, B. Tahir, Dynamic Photocatalytic Reduction of CO_2 to CO in a Honeycomb Monolith Reactor Loaded with Cu and N Doped TiO_2 Nanocatalysts, Appl. Surf. Sci, Vol. 377, 2016, pp. 244-252.

[7] I. Levchuk, M. Sillanpää, C. Guillard, D. Gregori, D. Chateau, S. Parola, TiO_2/SiO_2 Porous Composite Thin Films: Role of TiO_2 Areal Loading and Modification with Gold Nanospheres on the Photocatalytic Activity, Appl. Surf. Sci, Vol. 383, 2016, pp. 367-374.

[8] M. Pelaez, N. T. Nolan, S. C. Pillai, M. K. Seery, P. Falaras, A. G. Kontos, P. S. Dunlop, J. W. Hamilton, J. A. Byrne, K. O'shea, A Review on the Visible Light Active Titanium Dioxide Photocatalysts for Environmental Applications, Appl. Catal. B, Vol. 125, 2012, pp. 331-349.

[9] Z. He, J. Tang, J. Shen, J. Chen, S. Song, Enhancement of Photocatalytic Reduction of CO_2 to CH_4 Over TiO_2 Nanosheets by Modifying with Sulfuric Acid, Appl. Surf. Sci, Vol. 364, 2016, pp. 416-427.

[10] H. Xu, S. Ouyang, L. Liu, P. Reunchan, N. Umezawa, J. Ye, Recent Advances in TiO_2-

Based Photocatalysis, J. Mater. Chem. A, Vol. 2, 2014, pp. 12642-12661.

[11] G. T. Vuong, M. H. Pham, D. T. On, Engineering Porosity of MIL-88B Metal-Organic Framework, Dalton Trans, Vol. 42, 2013, pp. 550-557.

[12] L. M. Cam, L. V. Khu, N. T. T. Ha, N. N. Ha, Synthesis of FeCo-MIL-88B and Investigate Its Potential for CO_2 Capture, VNU Journal of Science: Natural Sciences and Technology, Vol. 35, 2019, pp. 1-8 (in Vietnamese).

[13] J. M. Soler, E. Artacho, J. D. Gale, Alberto García, Javier Junquera, Pablo Ordejón, Daniel Sánchez-Portal, The SIESTA Method for ab Initio Order-N Materials Simulation, J. Phys, Cond, Matt, Vol. 14, 2002, pp. 2745.

[14] J. P. Perdew, K. Burke, M. Ernzerhof, Generalized Gradient Approximation Made Simple, Phys. Rev. Let, Vol. 77, 1996, pp. 3865.

[15] K. S. W. Sing, D. H. Everett, R. A. W. Haul et al., Reporting Physisorption Data for Gas/Solid Systems with Special Reference to the Determination of Surface Area and Porosity, Pure Appl, Chem., Vol. 57, No. 4, 1985, pp. 603-619.

[16] H. Zangeneh , M. Farhadian , A. A. Zinatizadeh, A Reusable Visible Driven N and C-N Doped TiO_2 Magnetic Nanocomposites for Photodegradation of Direct Red 16 Azo Dye in Water and Wastewater, Environ, Technol, Vol. 43, No. 9, 2022, pp. 1269-1284.

[17] T. S. Natarajan, V. Mozhiarasi, R. J. Tayade, Nitrogen Doped Titanium Dioxide (N-TiO_2): Synopsis of Synthesis Methodologies, Doping Mechanisms, Property Evaluation and Visible Light Photocatalytic Applications, Photochem, Vol. 1, 2021, pp. 371-410.